PCCP

Accepted Manuscript

This is an *Accepted Manuscript*, which has been through the Royal Society of Chemistry peer review process and has been accepted for publication.

Accepted Manuscripts are published online shortly after acceptance, before technical editing, formatting and proof reading. Using this free service, authors can make their results available to the community, in citable form, before we publish the edited article. We will replace this *Accepted Manuscript* with the edited and formatted *Advance Article* as soon as it is available.

You can find more information about *Accepted Manuscripts* in the Information for Authors.

Please note that technical editing may introduce minor changes to the text and/or graphics, which may alter content. The journal's standard Terms & Conditions and the Ethical guidelines still apply. In no event shall the Royal Society of Chemistry be held responsible for any errors or omissions in this *Accepted Manuscript* or any consequences arising from the use of any information it contains.

ROYAL SOCIETY OF CHEMISTRY

www.rsc.org/pccp

Journal Name

RSCPublishing

ARTICLE

An advanced Ag-based photocatalyst $Ag_2Ta_4O_{11}$ with outstanding activity, durability and universality for removing organic dyes

Cite this: DOI: 10.1039/xoxxoooooox

Received ooth January 2014,
Accepted ooth January 2014

DOI: 10.1039/xoxxoooooox

www.rsc.org/

Hongjun Dong,[a,b] Jingxue Sun,[a] Gang Chen,*[a] Chunmei Li,[a] Yidong Hu,[a] and Chade Lv[a]*

Constructing Ag-based photocatalysts by the incorporation of Ag^+ ions into metal/nonmetal oxides for removing organic pollutants is a recently developed strategy, but overcoming their own photocorrosion still is a tremendous change. In this work, an advanced Ag-based photocatalyst $Ag_2Ta_4O_{11}$ is obtained by this strategy, which exhibits improved photocatalytic activity compared with Ta_2O_5 and the universality for degrading several organic dyes. Importantly, the $Ag_2Ta_4O_{11}$ photocatalyst has the outstanding durability and reusability, which implies that it has potential application prospects for organic wastewater treatment in the printing and dyeing industry.

Introduction

Energy and environmental problems have become an increasingly serious fact with the development of economy and industry. Dyes used in the modern printing and dyeing industry usually as major wastewater pollutants release into the ecological environment. Dyes not only interfere with the photosynthesis of aquatic plants in the water, but also many N-containing of them can yield potentially carcinogenic aromatic amines after natural reductive anaerobic degradation[1-2]. Therefore, the emphasizing conventional physics and chemistry methods in the past must shift to unconventional green routes to mineralize industrial dyes employing renewable energy sources.

As a green eco-friendly technique, photocatalysis has been regarded as an important field in the organic pollutant treatment.[3-5] Therefore, exploiting high-effective photocatalytic materials has become a hot topic and attached more and more attention because they can take full advantage of the inexhaustible solar energy. Since Frank et al. reports that TiO_2 can photocatalytic decompose ethanenitrile and cyanide anions in water,[6-7] all kinds of transition metal oxides as photocatalysts have been widely developed. Such as WO_3,[8] MnO_2,[9] Fe_2O_3[10] and Cu_2O,[11] ZnO,[12] et al. display the high-effective photodegradation ability for removing organic pollutants in water. In recent years, the incorporation of Ag^+ ions into metal/nonmetal oxides constructing Ag-based composite oxide photocatalysts has been evidenced to be an effective strategy for adjusting band structure and position of semiconductor to improve photocatalytic activity.[13] It mainly benefits from the unique filled d^{10} electronic configurations of Ag^+ ions taking part in composition and hybridization of energy band in the majority of Ag-based compounds.[13-18] In consequence, the goal-directed designing Ag-based composite oxides based on this strategy can adjust electronic structure and light absorption property of photocatalysts. Currently, the plenty of researches for Ag-based composite oxide photocatalysts come forth continuously, which display high-efficiency decomposing organic pollutants and O_2 evolution ability under light irradiation and are believed to be a kind of promising photocatalytic materials.[14-26] However, the durable operation of Ag-based photocatalyst are difficult to realize owing to their usually high photocorrosion feature. In fact, for all kinds of photocatalysts, it is the stability and durability that are very significant for their actual application. Up to now, avoiding and mitigating deactivation of Ag-based photocatalyst is still one major challenge. Although many methods such as doping,[18] loading[27] and constructing heterojunction[28] etc. have been developed to improve photocatalytic activity and stability of Ag-based photocatalysts, they no doubt increase the difficulty and complexity in the preparation and have not solved their deactivation problems fundamentally. Therefore, if we can exploit a kind of Ag-based photocatalyst that can maintain the long-term stable operation, the suffered deactivation may be conquered to the maximum degree.

Tantalum pentoxide (Ta_2O_5)[27] and its composite oxides[30] as photocatalysts usually have wide band gap and have been applied to H_2-production materials for water splitting extensively, but they are rarely used for degrading organic

Physical Chemistry Chemical Physics Accepted Manuscript

pollutants. Taking fully into account the incorporation effect of Ag^+ ions, in this work, the layer structured $Ag_2Ta_4O_{11}$ is prepared, which exhibits improved photocatalytic activity relative to Ta_2O_5 and the universality for degrading several organic dyes. The encouraging result is that the as-obtained $Ag_2Ta_4O_{11}$ photocatalyst achieves ultra-long durable operation, the activity of which for degrading MB almost has no reduction throughout circle experiments of 50 times enduring the cumulative 1000 min reaction.

Experimental

Synthesis and characterization

The sample was prepared by the solid state reaction method. The typical experimental procedure was that Ta_2O_5 (AR) and $AgNO_3$ (AR) were weighed out in terms of an appropriate stoichiometric ratio. The mixture was ground 30 min in a mortar so that it was homogeneous mixing, and then transferred into a corundum crucible and heated 4 h at 500 °C in an electric furnace in the air. The precursor was removed and vigorously ground for 30 min and calcined 24 h at 1000 °C. The final white $Ag_2Ta_4O_{11}$ product was achieved.

The phase of the sample was characterized by powder X-ray diffractometer (XRD, Rigaku D/max-2000) equipped with a Cu-Kα radiation at a scanning rate of 5° min^{-1} in the 2θ range of 10-90°. The morphology of sample was characterized utilizing field-emission scanning electron microscopy (FESEM, MX2600FESEM) and transmission electron microscopy (TEM, FEI, Tecnai G2 S-Twin). X-ray photoelectron spectroscopy (XPS) was measured on an American electronics physical HI5700ESCA system with X-ray photoelectron spectroscope using Al Kα (1486.6 eV) monochromatic X-ray radiation. The peak positions were corrected against the C 1s peak (284.6 eV) of contaminated carbon. The UV-visible diffuse reflectance spectrum (UV-vis DRS) of sample was recorded on a UV-vis spectrophotometer (PG, TU-1901) at room temperature with $BaSO_4$ as the background at 200-450 nm. The Brunauer-Emmett-Teller (BET) specific surface area was measured at 77 K using an AUTOSORB-1 Surface Area and Pore Size Analyzer. The photoluminescence (PL) spectrum was measured with a Perkin Elmer LS55 at room temperature.

Photocatalytic and photoelectrochemical measurements

The degradations of the organic dyes were carried out with 0.3 g $Ag_2Ta_4O_{11}$ and commercial Ta_2O_5 as comparison suspended in the methylene blue (MB), rhodamine B (RhB) or Methyl orange (MO) solutions (10 mg L^{-1}, 100 ml) with 0.1 ml H_2O_2. Then the degradation reaction system was irradiated with a 300W Xe arc lamp providing UV-visible light. Before the suspensions were irradiated, they were performed about 2 min of ultrasonic process and magnetically stirred for 30 min in the dark to complete the adsorption-desorption equilibrium between dye and photocatalyst. Lastly, the above suspensions were exposed to UV-visible light irradiation under magnetic stirring. UV-vis spectrophotometer (PG, TU-1901) monitored the absorbance of dye solution at intervals of 5 min. Before measurement, the photocatalyst was removed from the reaction system by centrifugalization.

The photoelectrochemical characteristics were measured in a CHI604C electrochemical working station using a standard three-compartment cell under UV-visible light. The FTO glasses (1cm×1cm) were washed 30 min using detergent, acetone and ethanol absolute under the ultrasound, respectively. The sample of 0.01g and terpilenol of 0.5 ml were put in agate mortar to ground 30 min. Then the obtained mixtures were coated on the FTO glasses using the spin coater with 4000 revolutions per minute. Lastly, the coated FTO glasses were performed drying 24 h at 80 °C. Photocatalyst coated FTO glass, a piece of Pt sheet, an Ag/AgCl electrode and 0.01 M sodium carbonate were used as the working electrode, counter-electrode, reference electrode and electrolyte, respectively.

Results and discussion

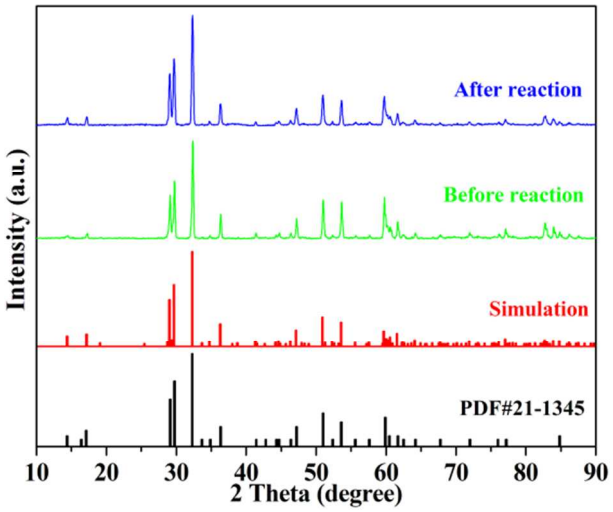

Fig. 1 XRD patterns of the $Ag_2Ta_4O_{11}$ sample before and after reaction.

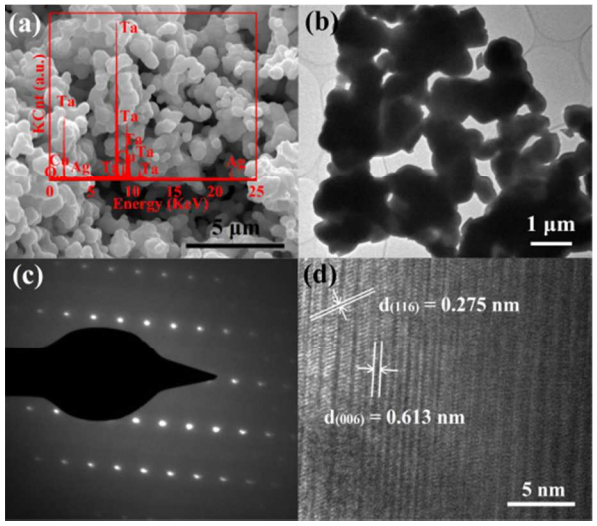

Fig. 2 SEM image (a), TEM image (b), SAED pattern (c) and HRTEM image (d) of the $Ag_2Ta_4O_{11}$ sample.

Physical Chemistry Chemical Physics Accepted Manuscript

This journal is © The Royal Society of Chemistry 2012

Fig. 1 shows XRD pattern of the $Ag_2Ta_4O_{11}$ sample before reaction, which agrees well with the simulated spectrum and standard spectrum (PDF#21-1345). There are not any other phases appearing, which indicates that the pure $Ag_2Ta_4O_{11}$ sample is obtained. In addition, the strong, narrow and sharp diffraction peaks imply that the sample has a well-crystallinity. The SEM image in Fig. 2a shows that the sample exhibits irregular bulk distribution, and the EDS spectrum (the insert of Fig. 2a) presents that the sample is composed of Ag, Ta and O elements. The TEM image (Fig. 2b) further reveals that these bulks are aggregated by the smaller particles (0.5-2 μm) by reason of the high-temperature calcination. Furthermore, the SAED is performed on the whole bulk (Fig. 2c), where the diffraction pattern shows distinctly symmetrical diffraction spots, which demonstrates that the sample displays single crystal characteristic. In addition, From the HRTEM image of the sample in Fig. 2d, the lattice fringe image shows that the marked interplanar spacing *d* is equal to 0.613 nm and 0.275 nm, which correspond to (006) and (116) crystal plane in hexagonal $Ag_2Ta_4O_{11}$ crystal, respectively. It further evidences that the pure $Ag_2Ta_4O_{11}$ sample is achieved.

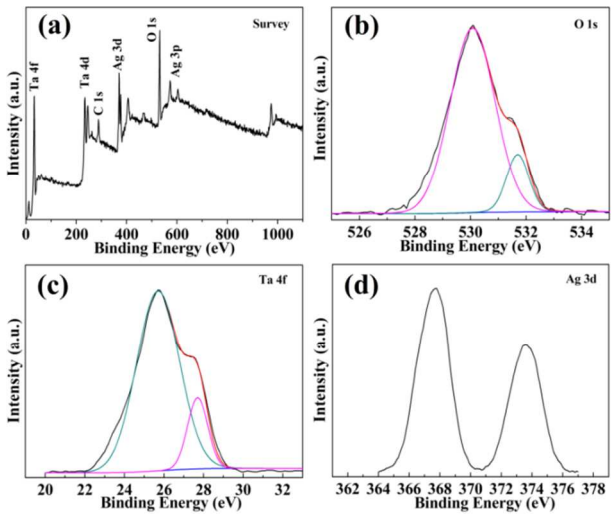

Fig. 3 XPS spectra of the $Ag_2Ta_4O_{11}$ sample, (a) survey, (b) O 1s, (c) Ta 4f, (d) Ag 3d

The XPS spectra of the $Ag_2Ta_4O_{11}$ sample are performed to investigate the surface elements and their valence states. The survey XPS spectrum in Fig. 3a identifies the sample is composed of Ag, Ta, and O elements, which is in accord with the results from EDS. From the oxygen XPS spectrum in Fig. 3b, there are two overlapped O 1s peaks, which implies that O has two different chemical states[31] arising from O^{2-} in the lattice of $Ag_2Ta_4O_{11}$ surface and the hydroxyl species from adsorbed contaminants at 530.1 and 531.7 eV, respectively.[32] In addition, Fig. 3c exhibits the obvious binding energy peaks at 25.7 and 27.7 eV, which attribute to $4f_{7/2}$ and $4f_{5/2}$ states of Ta^{5+} in the lattice of $Ag_2Ta_4O_{11}$ surface, respectively. Moreover, Fig. 3d show symmetrical binding energy peaks at 367.8 and 373.6 eV, respectively, which demonstrates that silver has only one chemical state deriving from $3d_{5/2}$ and $3d_{3/2}$ states of Ag^+ in the lattice of $Ag_2Ta_4O_{11}$ surface.[33]

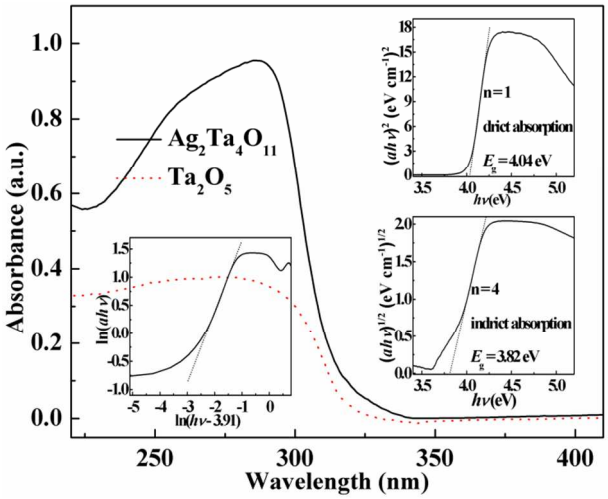

Fig. 4 UV-vis DRS spectrum of the $Ag_2Ta_4O_{11}$ and Ta_2O_5 sample, The insert are plots of $\ln(\alpha h\nu)$ vs $\ln(h\nu\text{-}3.95)$ and $(\alpha h\nu)^{n/2}$ vs $h\nu$ (n=1 or 4) for $Ag_2Ta_4O_{11}$.

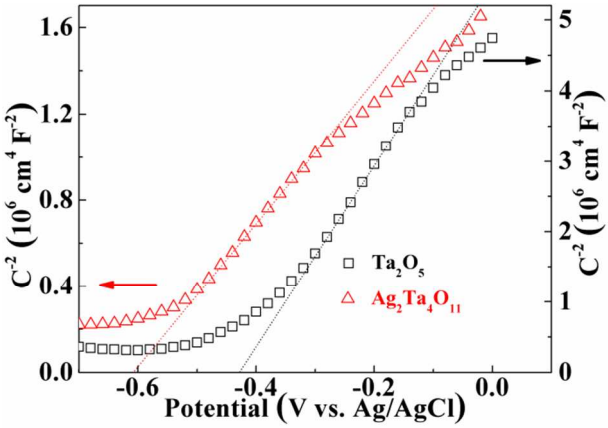

Fig. 5 Mott-Schottky plots of the $Ag_2Ta_4O_{11}$ and Ta_2O_5 electrodes

The UV-vis DRS spectra of the $Ag_2Ta_4O_{11}$ sample and Ta_2O_5 is performed to investigate the effect of Ag^+ ions incorporating into Ta_2O_5 on the light absorption ability of the photocatalyst. As shown in Fig. 4, the $Ag_2Ta_4O_{11}$ sample exhibits slight redshift relative to Ta_2O_5 and the steep absorption edge demonstrates that the strong light absorption stems from the intrinsic band gap transition of the sample instead of impurity levels. Moreover, the energy band edge and band transition mode of the $Ag_2Ta_4O_{11}$ sample are estimated using the empirical equations of the crystal semiconductor (ESI†). From the insert of Fig. 4, further analyzing plots of $\ln(\alpha h\nu)$ vs $\ln(h\nu\text{-}3.95)$ and $(\alpha h\nu)^{n/2}$ vs $h\nu$ (n=1 or 4) reveals that $Ag_2Ta_4O_{11}$ has an indirect band gap of 3.82 eV as well as a direct transition of 4.04 eV, respectively. The narrower indirect band gap of $Ag_2Ta_4O_{11}$ than that of Ta_2O_5 (4.0 eV)[29] is an important reason of the former presenting the higher phtotcatalytic activity. It originates that incorporation of Ag^+

Physical Chemistry Chemical Physics Accepted Manuscript

ions into Ta_2O_5 results in constructing the new crystal structure and energy band structure. In addition, the BET specific surface area of the $Ag_2Ta_4O_{11}$ sample is measured to be 0.9426 $m^2 g^{-1}$, which is slightly below that of the Ta_2O_5 sample (1.1405 $m^2 g^{-1}$), thus indicating that its effect on photodegradation activity can be negligible.

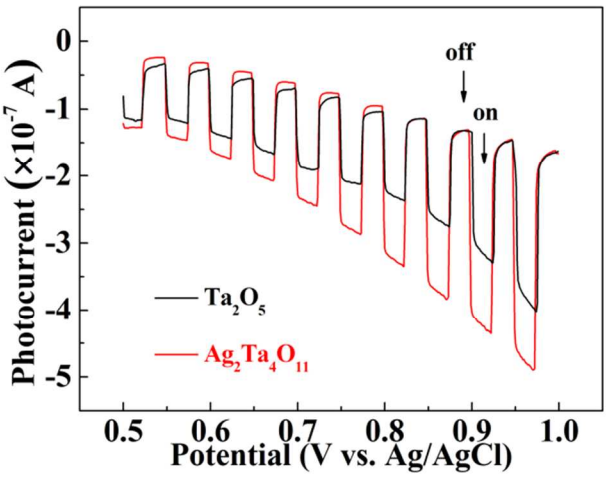

Fig. 6 Photocurrent responses of the $Ag_2Ta_4O_{11}$ and Ta_2O_5 electrodes.

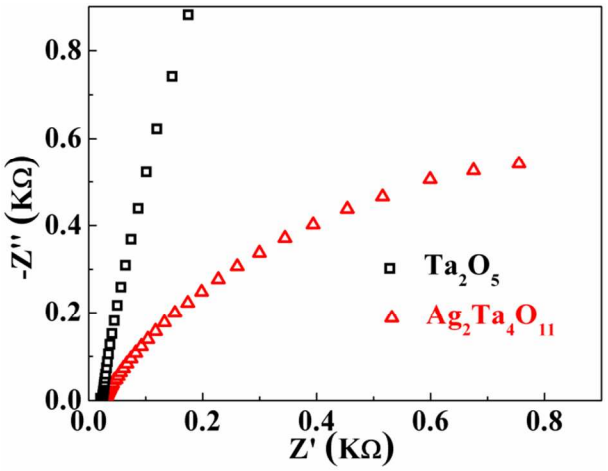

Fig. 7 EIS plots of the $Ag_2Ta_4O_{11}$ and Ta_2O_5 electrodes.

It has been reported that the photocatalytic reaction can be regarded as a photoelectrochemical process.[34-35] Therefore, Mott-Schottky plots are performed to understand the incorporation Ag^+ ions into Ta_2O_5 effecting on semiconducting properties. Mott-Schottky relationships on n-type and p-type semiconductors are described based on two equations (ESI†).[36-39] Fig. 5 shows the Mott-Schottky plots of the $Ag_2Ta_4O_{11}$ and Ta_2O_5 electrodes, respectively. There are the positive slopes in the linear region of their plots, indicating that they are n-type semiconductor. Furthermore, the flat-band potential of $Ag_2Ta_4O_{11}$ (-0.61 V) is higher 0.17 V than that of Ta_2O_5 (-0.44 V). The CB position of $Ag_2Ta_4O_{11}$ is more negative than that of Ta_2O_5 because the CB potential of n-type semiconductors is very close to the flat-band potential,[38] the variation trend of which is in accord with the calculated results using the empirical formulae (Table S1, ESI†). It implies that $Ag_2Ta_4O_{11}$ has more intense reducing capacity, which is beneficial to capturing H_2O_2 in water to yield more hydroxyl radical (HO·) activated species decomposing dyes.

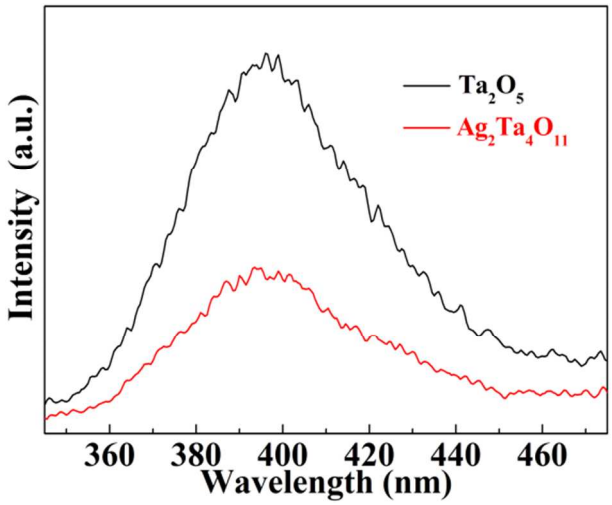

Fig. 8 PL spectra of the $Ag_2Ta_4O_{11}$ and Ta_2O_5 samples.

Generally, the value of photocurrent indirectly reflects the semiconductor's ability to generate and transfer the photogenerated charge carriers under light irradiation, which closely correlates with the photocatalytic activity. Fig. 6 shows the current density plots of the $Ag_2Ta_4O_{11}$ and Ta_2O_5 electrodes under UV-visible light. Ta_2O_5 electrode exhibits the photocurrent density of -4.0×10^{-7} A cm^{-2} at bias voltage of 0.97 V. By comparison, $Ag_2Ta_4O_{11}$ electrode yields an enhancive photocurrent density of -4.9×10^{-7} A cm^{-2} at the same applied voltage, which is nearly 1.23 times as much that of Ta_2O_5 electrode and produces a roughly increase of 22.5%. It indicates that the faster charge transfer and more effective separation of electron-hole pairs through the $Ag_2Ta_4O_{11}$ electrode interface,[39] which is evidenced by Electrochemical Impedance Spectroscopy (EIS). From the EIS spectra of $Ag_2Ta_4O_{11}$ and Ta_2O_5 electrodes in Fig. 7, the arc radius on the Nyquist plot of $Ag_2Ta_4O_{11}$ electrode is smaller than that of Ta_2O_5 electrode, which implies that the former has more high-efficiency charge transfer ability.[34-35] All above results reveal that the incorporation of Ag^+ into Ta_2O_5 also improve photoelectrochemical behavior of the photocatalyst in favor of enhancing photocatalytic activity. In addition, as far as semiconductor photocatalysts are concerned, the PL intensity is closely related to the transfer and separated behavior of the photogenerated charge carriers, so that it can also reflect the separation/recombination of electrons and holes to some extent. The PL spectra of the $Ag_2Ta_4O_{11}$ and Ta_2O_5 samples are shown in Fig. 8. It is evident that the PL intensity of the $Ag_2Ta_4O_{11}$ sample is lower than that of the Ta_2O_5 sample. The obvious fluorescence quenching for the $Ag_2Ta_4O_{11}$ sample relative to the Ta_2O_5 sample implies that the incorporation of Ag^+ into Ta_2O_5 gives rise to the lower recombination rate of charge carriers availing photocatalytic activity improvment.[40-41]

Physical Chemistry Chemical Physics Accepted Manuscript

This journal is © The Royal Society of Chemistry 2012

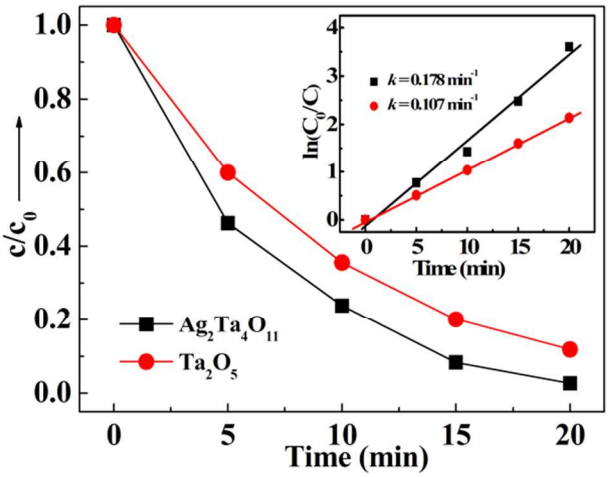

Fig. 9 Dynamic curves and plots of $\ln(c_0/c)$ versus time (insert) of MB solution over the $Ag_2Ta_4O_{11}$ and Ta_2O_5 samples under UV-visible light.

In order to research the effect of Ag^+ incorporation into Ta_2O_5 on photocatalytic activity, the RhB, MB and MO dyes as typical organic pollutants in textile printing wastewater are used for target molecules to evaluate the degradation ability of phtocatalysts. Fig. 9 shows the contrast of dynamic curves for MB degradation over the $Ag_2Ta_4O_{11}$ and Ta_2O_5 samples. After running 20 min, the removal rate of MB over the $Ag_2Ta_4O_{11}$ sample is more than 98%. In contrast, only 87% of MB is decomposed over the Ta_2O_5 sample under the same condition. Moreover, the photodegradation kinetic curves of MB degradation can be approximated as a pseudo-first-order process.[42] By plotting the $\ln(c_0/c)$ versus time and making linear fitting for kinetic curves of MB solutions (in the insert of Fig.. 9), the removal rate constant k of MB over the $Ag_2Ta_4O_{11}$ sample is estimated to be 0.178 min^{-1}, which amazingly reaches to ~1.66 times as much as that over the Ta_2O_5 sample (0.107 min^{-1}). Furthermore, as can be seen from the absorbance variations of MB solution in the photocatalytic reaction (Fig. 10), there is not shifting of the maximum absorption wavelength position of MB solution at 663 nm and the absorption peak at 292 nm vanishes in ultraviolet region besides that in visible region. It implies that the benzene/heterocyclic rings of MB molecule may be decomposed completely, leading to the thorough mineralization of MB,[17] which is further proved by total organic carbon (TOC) variation in solutions (Fig. S1). The similar results of photocatalytic activity improvement are further evidenced *via* the degradation of RhB and MO dyes. As shown in Fig. S2-S3 (ESI†), the degradation rates of the RhB and MO dyes achieve 97% and 88% after 20 and 35 min over the $Ag_2Ta_4O_{11}$ sample, which are higher that of 86% and 62% over the Ta_2O_5 sample, respectively. Meanwhile, the absorbance of RhB and MO solutions in both the visible and ultraviolet regions are also dying down (Fig. S4-S5, ESI†), which suggests the complete mineralization of them. In addition, the photodegradation activity of $Ag_2Ta_4O_{11}$ is also higher than that of P25 and ZnO (Fig. S6). Furthermore, the circle operation experiments of degrading MB are carried out to estimate durability and reusability of the $Ag_2Ta_4O_{11}$ sample (Fig. 11). The photocatalytic activity of the $Ag_2Ta_4O_{11}$ sample exhibits no distinct loss after 50 recycle operations undergoing cumulative 1000 min reaction. The removal rate still achieves 94% within 20 min in the last 50th circle. Meanwhile, it is worth noting that the XRD pattern of the used sample after reaction in Fig. 1 is nearly unchanged and no new phases are detected, which demonstrates that the $Ag_2Ta_4O_{11}$ sample is a relatively stable Ag-based photocatalyst. These results demonstrate that the photodegratation activity of the $Ag_2Ta_4O_{11}$ photocatalyst is obvious superior to that of Ta_2O_5, as well as the $Ag_2Ta_4O_{11}$ photocatalyst has the universality for degrading various organic dyes and exhibits the outstanding durability and reusability.

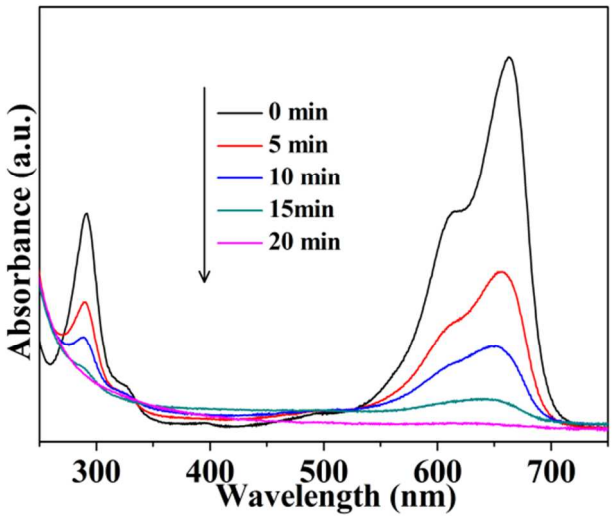

Fig. 10 Absorbance variations of MB solution over the $Ag_2Ta_4O_{11}$ sample under UV-visible light.

The transfer and separation behavior of charge carriers and dye photodegradation mechanism over the $Ag_2Ta_4O_{11}$ sample is illustrated in Scheme 1. Under the UV-visible light irradiation, the electrons and holes are yielded in $Ag_2Ta_4O_{11}$ crystal, and then transfer to the surface to participate in redox reactions in photodegradation process, respectively. Furthermore, the theoretical calculation based on ab initio density functional theory reveals that the CB and VB of $Ag_2Ta_4O_{11}$ mainly consist of the Ta 5d orbital and hybridized Ag 4d and O 2p orbital, respectively.[43] In addition, as a typical layer-structured compound similar to $Ag_2Nb_4O_{11}$, $Ag_2Ta_4O_{11}$ is composed of AgO_6 octahedrons, TaO_6 octahedrons and TaO_7 pentagonal bipyramids,[35] which can build an interlaced three dimensional framework in the crystal structure. This unique electronic and crystal structure is conducive to transfer and separation of charge carriers inside crystal. Once the $Ag_2Ta_4O_{11}$ sample is irradiated by the UV-visible light, the electron-hole pairs are firstly generated on AgO_6 octahedrons. The electrons then immediately migrate to surrounding TaO_6 octahedrons and TaO_7 pentagonal bipyramids. Subsequently, the electrons in TaO_6 octahedrons and TaO_7 pentagonal bipyramids exposed to

Physical Chemistry Chemical Physics Accepted Manuscript

the crystal surface quickly are captured by H_2O_2 to produce HO• decomposing dyes. In the meantime, the holes in exposed AgO_6 octahedrons on the crystal surface also directly oxidize dyes. The result of exporting electrons from AgO_6 octahedrons not only separates effectively electron-hole pairs to improve photodegradation activity, but also further enhances the stability of the $Ag_2Ta_4O_{11}$ sample owing to relieving reduction of Ag^+ ions in crystal lattices.

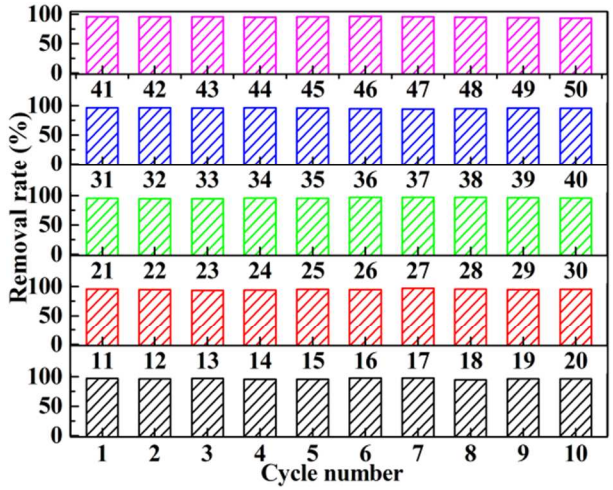

Fig. 11 Removal rates of the MB after each of circle operations reacting 20 min over the $Ag_2Ta_4O_{11}$ sample.

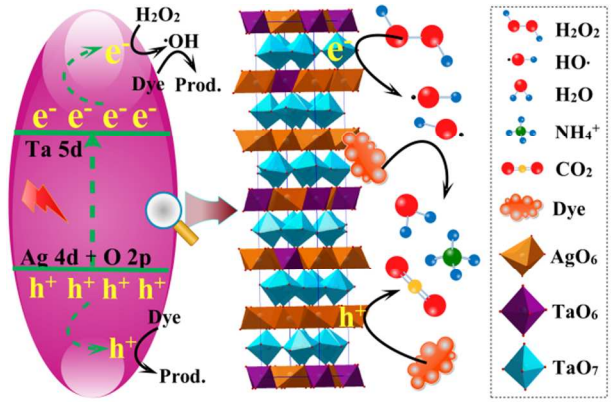

Scheme 1 Transfer and separation behaviour of charge carriers and dye photodegradation mechanism over the $Ag_2Ta_4O_{11}$ sample.

Conclusions

In summary, an advanced Ag-based photocatalyst $Ag_2Ta_4O_{11}$ is achieved on the basis of the strategy of incorporating Ag^+ ions into transition metal oxide Ta_2O_5. The light absorption, photoelectrochemical and photoluminescent characteristics reveal that the improved photocatalytic activity for removing organic dyes mainly attributes to widening light harvest range, enhancing reduction ability and increasing separated efficiency of charge carriers, which results from the incorporation effect of Ag^+ ions. More importantly, the $Ag_2Ta_4O_{11}$ photocatalyst exhibits the universality for degrading several organic dyes and ultralong durable operation of cumulative 1000 min throughout circle experiments of 50 times. Therefore, the $Ag_2Ta_4O_{11}$ photocatalyst has the outstanding activity, durability and reusability, which has potential application prospects for organic wastewater treatment in the printing and dyeing industry.

Acknowledgements

This work was financially supported by the National Nature Science Foundation of China (21071036, 21271055 and 21471040) and Province Natural Science Foundation of Heilongjiang Province (ZD201011). We acknowledge for the support by Open Project of State Key Laboratory of Urban Water Resource and Environment, Harbin Institute of Technology (No. QAK201304) and Program for Innovation Research of Science in Harbin Institute of Technology.

Notes and references

[a] Department of Chemistry, Harbin Institute of Technology, Harbin 150001, P. R. China.
[b] Department of Chemistry, Baicheng Normal University, Baicheng 137000, P. R. China.
E-mail: gchen@hit.edu.cn, skybluesnow@163.com, Fax: (+86)-451-86413753

† Electronic Supplementary Information (ESI) available: See DOI: 10.1039/b000000x/

1. S. Horikoshi, F. Hojo, H. Hikaka and N. Serpone, *Environ. Sci. Technol.*, 2004, **38**, 2198-2208.
2. N. Z. Bao, X. Feng, Z. H. Yang, L. M. Shen and X. H. Lu, *Environ. Sci. Technol.*, 2004, **38**, 2729-2736.
3. A. Y. Zhang, L. L. Long, C. Liu, W. W. Li and H. Q. Yu, *Green Chem.*, 2014, **16**, 2745-2753.
4. C. Chen, W. Ma and J. Zhao, *Chem. Soc. Rev.*, 2010, **39**, 4206-4219.
5. H. Guo, Y. Guo, L. Liu, T. Li, W. Wang, W. Chen and J. Chen, *Green Chem.*, **2014**, *16*, 2539-2545.
6. S. N. Fran and A. J. Bard, *J. Am. Chem. Soc.*,1975, **97**, 7427-7433.
7. S. N. Fran and A. J. Bard, *J. Am. Chem. Soc.*, 1977, **99**, 303-304.
8. F. Amano, E. Ishinaga and A. Yamakata, *J. Phys. Chem. C*, 2013, **117**, 22584-22590.
9. M. L. Chacón-Patiño, C. Blanco-Tirado, J. P. Hinestroza and M. Y. Combariza, *Green Chem.*, 2013, **15**, 2920-2928.
10. W. Sun, Q. Meng, L. Jing, D. Liu and Y. Cao, *J. Phys. Chem. C*, 2013, **117**, 1358-1365.
11. L. Zhang, J. Shi, M. Liu, D. Jing and L. Guo, *Chem. Commun.*, 2014, **50**, 192-194.
12. A. P. Bhirud, S. D. Sathaye, R. P. Waichal, L. K. Nikam and B. B. Kale, *Green Chem.*, 2012, **14**, 2790-2798.
13. T. Kako, N. Kikugawa and J. Ye, *Catal. Today*, 2008, **131**, 197-202.
14. Z. G. Yi, J. H. Ye, N. Kikugawa, T. Kako, S. X. Ouyang, H. Stuart-Williams, H. Yang, J. Y. Cao, W. J. Luo, Z. S. Li, Y. Liu and R. L. Withers, *Nat. Mater.*, 2010, **9**, 559-563.
15. J. W. Tang, Z. G. Zou and J. H. Ye, *J. Phys. Chem. B*, 2003, **107**, 14265-14269.
16. R. Konta, H. Kato, H. Kobayashi and A. Kudo, *Phys. Chem. Chem. Phys.*, 2003, **5**, 3061-3065.

Physical Chemistry Chemical Physics Accepted Manuscript

This journal is © The Royal Society of Chemistry 2012

17. H. J. Dong, G. Chen, J. X. Sun, C. M. Li, Y. G. Yu and D. H. Chen, *Appl. Catal. B: Environ.*, 2013, **134-135**, 46-54.
18. X. K. Li, S. X. Ouyang, N. Kikugawa and J. H. Ye, *Appl. Catal. A: Gen.*, 2008, **334**, 51-58.
19. S. X. Ouyang and J. H. Ye, *J. Am. Chem. Soc.*, 2011, **133**, 7757-7763.
20. Y. P. Bi, H. Y. Hu, S. X. Ouyang, G. X. Lu, J. Y. Cao and J. H. Ye, *Chem. Commun.*, 2012, **48**, 3748-3750.
21. Y. X. Tang, Z. L. Jiang, G. C. Xing, A. R. Li, P. D. Kanhere, Y. Y. Zhang, T. C. Sum, S. Z. Li, X. D. Chen, Z. L. Dong and Z. Chen, *Adv. Funct. Mater.*, 2013, **23**, 2932-2940.
22. Y. S. Xu and W. D. Zhang, *ChemCatChem*, 2013, **5**, 2343-2351.
23. J. T. Tang, Y. H. Liu, H. Z. Li, Z. Tan and D. T. Li, *Chem. Commun.*, 2013, **49**, 5498-5500.
24. C. Hu, T. W. Peng, X. X. Hu, Y. L. Nie, X. F. Zhou, J. H. Qu and H. He, *J. Am. Chem. Soc.*, 2010, **132**, 857-862.
25. P. Wang, B. Huang, Y. Daiaand M. H. Whangbob, *Phys. Chem. Chem. Phys*., 2012, **14**, 9813-9825.
26. Z. Lou, B. Huang, Z. Wang, X. Ma, R. Zhang, X. Zhang, X. Qin, Y. Dai and M. H. Whangbo, *Chem. Mater*., 2014, **26**, 3873-3875.
27. L. Ni, M. Tanabe and H. Irie, *Chem. Commun.*, 2013, **49**, 10094-10096.
28. H. Dong, G. Chen, J. Sun, Y. Feng, C. Li, G Xiong, C. Lv, *Dalton Trans.*, 2014, **43**, 7282-7289.
29. Y. Takahara, J. N. Kondo, T. Takata, D. L. Lu and K. Domen, *Chem. Mater.*, 2001, **13**, 1194-1199.
30. Y. X. Li, L. Zang, Y. Li, Y. Liu, C. Y. Liu, Y. Zhang, H. Q. He and C. Y. Wang, *Chem. Mater.*, 2013, **25**, 2045-2050.
31. M. T. Uddin, Y. Nicolas, C. Olivier, T. Toupance, L. Servant, M. M. Müller, H. J. Kleebe, J. Ziegler and W. Jaegermann, *Inorg. Chem.*, 2012, **51**, 7764-7773.
32. J. B. Mu, C. L. Shao, Z. C. Guo, Z. Y. Zhang, M. Y. Zhang, P. Zhang, B. Chen and Y. C. Liu, *ACS Appl. Mater. Interfaces*, 2011, **3**, 590-596.
33. H. Dong, G. Chen, J. Sun, Y. Feng, C. Li and C. Lv, *Chem. Commun.*, 2014, **50**, 6596-6599.
34. Z. H. Zhang, R. Dua, L. B. Zhang, H. B. Zhu, H. G. Zhang and P. Wang, *ACS Nano.*, 2013, **7**, 1709-1717.
35. Q. W. Huang, S. Q. Tian, D. W. Zeng, X. X. Wang, W. L. Song, Y. Y. Li, W. Xiao and C. S. Xie, *ACS Catal.*, 2013, **3**, 1477-1485.
36. S. U. M. Khan and J. Akikusa, *J. Phys. Chem. B*, 1999, **103**, 7184-7189.
37. Z. Wu, G. Zhao, Y. Zhang, H. Tian and D. Li, *J. Phys. Chem. C*, 2012, **116**, 12829-12835.
38. M. Sun, G. D. Chen, Y. K. Zhang, Q. Wei, Z. M. Ma and B. Du, *Ind. Eng. Chem. Res.*, 2012, **51**, 2897-2903.
39. Y. H. Ng, I. V. Lightcap, K. Goodwin, M. Matsumura and P. V. Kamat, *J. Phys. Chem. Lett.*, 2010, **1**, 2222-2227.
40. Y. T. Liang, B. K. Vijayan, O. Lyandres, K. A. Gray and M. C. Hersam, *J. Phys. Chem. Lett.*, 2012, **3**, 1760-1765.
41. C. Y. Yang, Z. Wang, T. Q. Lin, H. Yin, X. J. Lü, D. Y. Wan, T. Xu, C. Zheng, J. H. Lin, F. Q. Huang, X. M. Xie and M. H. Jiang, *J. Am. Chem. Soc*., 2013, **135**, 17831-17838.
42. I. K. Konstantinou and T. A. Albanis, *Appl. Catal. B: Environ.*, 2004, **49**, 1-14.
43. J. Boltersdorf, T. Wong and P. A. Maggard, *ACS Catal.*, 2013, **3**, 2943-2953.

Physical Chemistry Chemical Physics Accepted Manuscript